Influence of terrestrial ecosystems and topography on coastal CO_2 measurements: A case study at Trinidad Head, California

W. J. Riley,[1] J. T. Randerson,[2] P. N. Foster,[3] and T. J. Lueker[4]

Received 20 December 2004; revised 6 April 2005; accepted 8 June 2005; published 7 September 2005.

[1] Coastal stations are critical for interpretation of continental-scale CO_2 exchanges although the impacts of land and sea breezes, local topography, katabatic winds, and CO_2 transport from nearby terrestrial ecosystems are not well characterized. We applied a modeling framework that couples meteorological (MM5), land-surface (LSM1), and tracer models to investigate the impact of these factors on coastal CO_2 measurements. Model predictions compared well with measurements over 4 months at our case study site (Trinidad Head, California). We predicted that during midday and under strong onshore wind conditions, positive and negative CO_2 anomalies from the assumed ''background'' marine layer air were sampled at the station. These anomalies resulted from two classes of mechanisms that couple transport and recent terrestrial ecosystem exchanges. First, and most important, are local and large-scale recirculation of nighttime positive CO_2 anomalies resulting from katabatic flows off the coastal mountain range. Second, negative anomalies generated by daytime net ecosystem uptake can be transported offshore in the residual layer and then entrained in the marine boundary layer. We predicted monthly averaged CO_2 anomalies associated with terrestrial exchanges of 0.53, 0.34, 3.1, and 0.05 ppm during March, June, September, and December of 2002. Positive anomalies from nighttime ecosystem respiration were more likely to be sampled than are negative anomalies associated with daytime net ecosystem uptake. Current atmospheric models used in continental-scale inverse studies do not resolve these two classes of mechanisms and therefore may infer incorrect CO_2 exchange rates.

Citation: Riley, W. J., J. T. Randerson, P. N. Foster, and T. J. Lueker (2005), Influence of terrestrial ecosystems and topography on coastal CO_2 measurements: A case study at Trinidad Head, California, *J. Geophys. Res.*, *110*, G01005, doi:10.1029/2004JG000007.

1. Introduction

[2] Evidence for a large Northern Hemisphere carbon sink depends largely on observations of the inter-hemispheric difference of atmospheric CO_2 measured with flasks at surface stations distributed in many remote locations, including coastal sites on continents and on ocean islands [*Tans et al.*, 1990; *Gurney et al.*, 2002]. Within the Northern Hemisphere, CO_2 concentrations from these stations upwind and downwind of continental regions have also been used, in part, to quantify the size of carbon sinks in North America [*Fan et al.*, 1998; *Gurney et al.*, 2002] and Europe [*Gurney et al.*, 2002; *Janssens et al.*, 2003].

[3] Observation and modeling studies have improved our understanding of diurnal and synoptic variability of surface CO_2 fluxes and atmospheric CO_2 concentrations above terrestrial ecosystems [*Yi et al.*, 2001; *Chou et al.*, 2002; *Denning et al.*, 2003; *Saleska et al.*, 2003; *Helliker et al.*, 2004]. However, much less is known about how terrestrial ecosystem fluxes interact with meteorology in the coastal domain to influence surface CO_2 concentrations. As a result, even though coastal observation stations continue to play a key role in both continental and hemispheric carbon source and sink partitioning studies, the effects of sea and land breezes, local topography, and katabatic winds are not well characterized. Flasks are opened in the middle of the day when winds are blowing onshore and when wind speed is above a minimum threshold (typically 2 m s^{-1}) to avoid impacts of nearby terrestrial ecosystem sources and sinks. Many of these coastal sampling locations are near substantial topographic discontinuities, such as coastal bluffs and coastal mountain ranges [*Conway et al.*, 1994]. Global transport models do not resolve these topographic features, nor the recirculation of CO_2 produced from nearby ecosystems that is entrained within the sea and land breezes. We hypothesize that global atmospheric models that fail to resolve mixing near the coast may introduce biases when used to predict CO_2 sources and sinks.

[4] *Goldstein et al.* [2004] reported results from a component of the NOAA Intercontinental Transport and Chemical Transformation 2002 (ITCT 2K2) study conducted at Trinidad Head, California. They concluded that variability

[1]Earth Sciences Division, E.O. Lawrence Berkeley National Laboratory, Berkeley, California, USA.
[2]Earth System Science Department, University of California, Irvine, California, USA.
[3]Department of Earth Sciences, University of Bristol, Bristol, UK.
[4]Geosciences Research Division, Scripps Institution of Oceanography, La Jolla, California, USA.

0148-0227/05/2004JG000007

in CO concentrations at this coastal sampling station was dominated by North America emissions. *Millet et al.* [2004], reporting on the same study, used factor analysis with measurements of speciated volatile organic compounds to quantify local versus global sources. Of the five factors they identified, three of them (accounting for 43% of the variance in their data set) were related to local sources and meteorology.

[5] The air quality community has studied the coupled impacts of land-surface sources and sinks, secondary pollutant formation, and coastal meteorology on atmospheric trace-gas concentrations. For example, *Lu and Turco* [1994] used a two-dimensional atmospheric model to characterize air pollutant transport in several generic coastal environments. They observed that pollutant transport is strongly influenced by topography and that sea breezes (i.e., onshore flow) and upslope flows during daytime heating in the mountains create vertical transport that can lead to increased concentrations in elevated atmospheric layers. In the return circulation (i.e., the land breeze that occurs at these higher altitudes), the tracer can be advected out over the ocean, where it may be entrained into the low-level onshore flow. In a follow-on study, *Lu and Turco* [1995] simulated three-dimensional flow and tracer transport over the Los Angeles Basin. In addition to observing patterns similar to those in their two-dimensional simulations, they described the impacts of horizontal convergence zones where pollutants can be injected into the free troposphere.

[6] *Lalas et al.* [1983] studied, on two typical days in Athens, well-defined sea-breeze circulations and pollutant transport. They concluded from ground-level trajectories and nighttime O_3 measurements that pollutants can be recirculated by land and sea breezes, and that this feature must be included in atmospheric chemistry modeling. They also observed multiple inversion layers, with different pollutant concentrations, in the air basin. Analogous vertical pollution layers have been observed in the Los Angeles air basin [*Lea*, 1968; *Edinger et al.*, 1972; *Edinger*, 1973; *Blumenthal et al.*, 1978] and along the California coast [*McElroy and Smith*, 1986, 1991].

[7] Because the emphasis in air quality has been on daytime sources, less attention has been paid to katabatic transport associated with nighttime radiative cooling of mountain slopes. However, katabatic flows and interactions with mountain waves occur regularly in coastal ranges. *Banta et al.* [1997] described the cleansing impact of nighttime downslope flows on atmospheric O_3 concentrations in a valley. *Fitzjarrald* [1986] discussed a study of anabatic and katabatic winds in central Veracruz state, Mexico. He concluded that the slow reversal of boundary layer winds may return air parcels to their initial starting altitude, and that this feature may be important for air pollution forecasting. *Manins* [1992] presented a model of the typical development of katabatic flow on a slope. After the sun sets, surface radiative cooling creates a layer of cold air near the surface. Turbulent transport of that cold air upward and long-wave radiative cooling of the air aloft create an inversion. A pressure gradient along the slope develops because the air near the surface is colder and denser than air at the same height in the free atmosphere. This pressure gradient forces a downslope jet with maximum wind speeds in the middle third of the inversion. Katabatic flows can be unsteady, and *Poulos and Bossert* [1995] argued that this variability can make pollutant dispersion predictions difficult.

[8] *Poulos et al.* [2000] presented observations and simulations describing the interactions of katabatic flows and mountain waves. Mountain waves, or topographically induced internal gravity waves, result when flow in a stable atmosphere is diverted away from its original path perpendicular to the barrier. They concluded that, generally, the existence of mountain wave flow reduces the opposing upstream-side katabatic flow that would otherwise exist in quiescent conditions, although the interaction is nonlinear. On the leeward side of the mountain the mountain wave flow augments the katabatic winds. Since these interactions strongly impact local wind fields, they will also affect CO_2 transport and atmospheric concentrations.

[9] The strong diurnal cycle of katabatic offshore and onshore winds is in phase with the diurnal cycle of positive and negative ecosystem CO_2 exchanges (positive CO_2 flux is defined toward the atmosphere). This phasing occurs because the external forcing for the local winds and CO_2 fluxes are, to first order, the same: incoming solar radiation and soil, plant, and air temperatures. During the day, photosynthetic uptake is often larger than respiratory sources, resulting in a net negative CO_2 ecosystem flux. At night, ecosystem respiration results in a net positive CO_2 flux to the atmosphere in phase with the potential for transport by katabatic offshore winds.

[10] To investigate the interactions between terrestrial CO_2 exchanges, local wind fields, and coastal CO_2 concentration measurements, we apply here a modeling framework that includes a coupled version of MM5 and LSM1 [*Cooley et al.*, 2005] and an atmospheric tracer transport model incorporated into MM5. The MM5-LSM1 model provides consistent predictions of net ecosystem CO_2, latent energy, and sensible energy exchanges at high spatial and temporal resolutions. We have successfully tested MM5-LSM1 against 3 years of surface measurements made during the FIFE campaign [*Cooley et al.*, 2005]. We also used the model to investigate the impact of land-use change on regional surface fluxes and near-surface climate [*Cooley et al.*, 2005] and to identify optimum locations for CO_2 measurements in California in order to quantify spatially distributed CO_2 sources and sinks [*Fischer et al.*, 2004].

[11] With this modeling framework, we assess the impacts of co-variation between NEE and coastal meteorological processes on CO_2 surface concentrations at a representative coastal site: Trinidad Head, California. Specifically, we investigate impacts on coastal surface CO_2 concentrations of land and sea breezes, katabatic flows, alongshore transport of CO_2 from adjacent ecosystems north and south of Trinidad Head, and re-introduction of lofted negative CO_2 anomalies into the marine boundary layer. We chose the Trinidad Head sampling station because (1) it is an important western boundary condition for continental U.S. carbon source and sink inversions; (2) it has many of the topographic features found at coastal stations; and (3) continuous O_2/N_2 and CO_2 measurements have been made at the station since October 1999 by the Atmospheric Oxygen Research Group (AORG) at the Scripps Institution of Oceanography [*Lueker et al.*, 2001].

[12] Diurnal variations in measured CO_2 concentrations at the Trinidad Head station can be large (e.g., up to 35 ppm in September); from these variations alone one might conclude that the station is inappropriate for sampling marine background air. However, as described below, samples are taken in the middle of the day when onshore winds are strong, and these conditions are assumed to result in air that has not recently been impacted by terrestrial ecosystems.

2. Methods

[13] We performed simulations of CO_2 samples at Trinidad Head, California using a coupled modeling framework that integrates MM5 [*Grell et al.*, 1995], LSM1 [*Bonan*, 1996], and a model for inert tracers in the atmosphere. In this section we briefly describe the model components and their integration.

[14] Trinidad Head is a prominent rock outcrop (~120 m elevation) about halfway between San Francisco, California, and Portland, Oregon, on the western coast of the United States (41.05°N, 124.15°W). Since 1995 the site has served continuously as a background air observatory to monitor trace gases for the Advanced Global Atmospheric Gases Experiment (AGAGE) [*Prinn et al.*, 2000], and is the site of continuing observations by NOAA (http://www.cmdl.noaa.gov/aero/net/thd/) and the Scripps Institution of Oceanography [*Lueker et al.*, 2001, 2003].

2.1. Modeling Framework

[15] MM5 [*Grell et al.*, 1995] is a nonhydrostatic, terrain-following sigma-coordinate mesoscale meteorological model used in weather forecasting and in studies of atmospheric dynamics, surface and atmosphere coupling, pollutant dispersion, etc. Many studies have tested or applied the model in a variety of terrains, including areas of complex topography and heterogeneous land-covers (for a partial list: http://www.mmm.ucar.edu/mm5/Publications/mm5-papers.html). The model can be run with nested grids so that large-scale atmospheric features can be captured as well as impacts of finescale topography and surface fluxes. The following physics packages were used in the simulations presented here: Grell convective scheme, simple ice microphysics, MRF PBL scheme, and the CCM2 radiation package. The MRF PBL scheme [*Hong and Pan*, 1996] is a high-resolution PBL transport model that includes both local and non-local vertical transport and has been applied and tested in many studies (see above list).

[16] LSM1 [*Bonan*, 1996] is a "big-leaf" [e.g., *Dickinson et al.*, 1986; *Sellers et al.*, 1996] land-surface model that simulates CO_2, H_2O, and energy fluxes between ecosystems and the atmosphere. Modules are included that simulate aboveground fluxes of radiation, momentum, sensible heat, and latent heat; and energy and water fluxes below ground, and coupled CO_2 and H_2O exchange between soil, plants, and the atmosphere. Twenty-eight surface types, comprising varying fractional land covers of 13 plant types, are simulated in the model. Soil hydraulic characteristics are determined from sand, silt, and clay content. LSM1 has been tested in a range of ecosystems at the site level [e.g., *Bonan et al.*, 1997, 1995; *Riley et al.*, 2003].

[17] The integration of LSM1 with MM5 was accomplished via the established interface for the OSULSM [*Chen and Dudhia*, 2001a, 2001b], with changes in the interface to account for partitioning shortwave radiation between diffuse and direct components. We have successfully tested the coupled atmospheric and land-surface model's predictions of surface latent heat fluxes, surface sensible heat fluxes, ground heat fluxes, near-surface air temperatures, soil temperature, and soil moisture by comparing predictions to data collected during the FIFE campaign [*Betts and Ball*, 1998; *Cooley et al.*, 2005]. In the analysis presented here we focus on the transport of CO_2 from local terrestrial ecosystems. We do not include fossil fuel sources because they are small within the model domain and because they probably do not contribute substantially to synoptic scale CO_2 variability at this remote site.

[18] The inert tracer model follows the current MM5 transport calculations for water vapor. Therefore, with respect to transport, CO_2 moves in the atmosphere with the same mechanisms as water vapor (e.g., turbulent transport in the mixed layer, convection). The land-surface CO_2 flux boundary condition was forced with net ecosystem CO_2 exchange (NEE) as predicted by LSM1.

[19] We imposed atmospheric CO_2 boundary conditions at the edges of the largest domain that were constant in time and space to allow us to isolate the impact of terrestrial ecosystem CO_2 exchange within the model domain on surface CO_2 measurements near the coast. All CO_2 concentration anomalies (ΔCO_2 (ppm)) are presented relative to this "background" boundary condition value. In reality, there is a substantial vertical gradient in CO_2 concentration over land and, to a lesser extent, over the ocean caused largely by remote fossil fuel emissions and seasonal terrestrial biosphere exchange [*Gerbig et al.*, 2003; *Olsen and Randerson*, 2004].

[20] We tested the tracer predictions by imposing boundary conditions and surface fluxes that were a set fraction of the water vapor concentrations and fluxes. We then verified that the predicted tracer fields remained in a consistent ratio with water vapor concentrations over a 4-week simulation. We also tested for numerical inaccuracies by imposing constant atmospheric CO_2 boundary conditions and no net surface exchanges, and verified that the predicted atmospheric concentrations did not change by more than 0.02 ppm over a 4-week simulation. Finally, we present below a comparison of predicted and measured CO_2 concentrations at the Trinidad Head station.

2.2. Simulations

[21] Four 1-month-long (March, June, September, and December) simulations for 2002 were performed. Although a full year was not simulated owing to computational constraints, these months represent a realistic range of meteorological conditions and ecosystem CO_2 exchanges over the year. We used the standard initialization procedure for MM5v3.5, which applies first-guess and boundary condition fields interpolated from the NCEP reanalysis data [*Kalnay et al.*, 1996; *Kistler et al.*, 2001] to the outer computational grid. The model was run with three one-way nested domains with horizontal resolutions of 36, 12, and 4 km (domains 1, 2, and 3, respectively, Figure 1). Domains 1, 2, and 3 had horizontal dimensions of 1080 × 1080, 144 × 144, and 52 × 52 km, respectively. Eighteen vertical sigma layers between the surface and 5000 Pa were

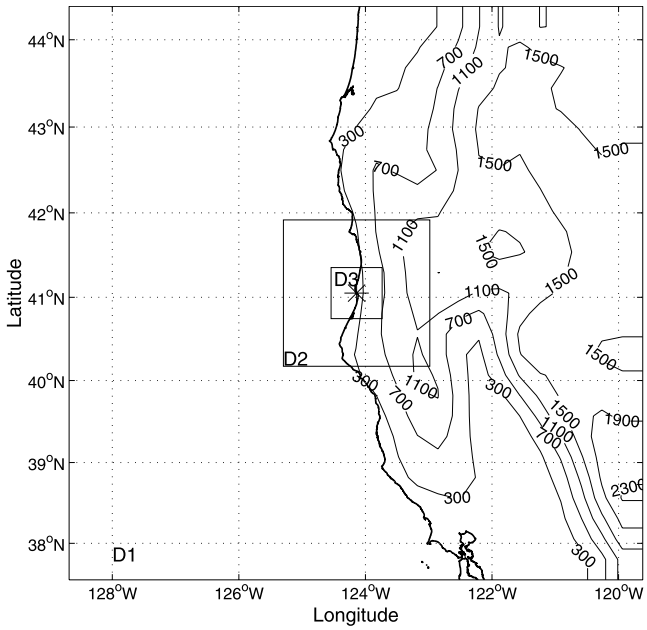

Figure 1. The three nested grids and terrain height (m) used in the simulations. The Trinidad Head, California, station (41.05°N, 124.15°W) shown with an asterisk. Domains 1, 2, and 3 (D1, D2, and D3) have horizontal resolutions of 36 km, 12 km, and 4 km, respectively, and horizontal dimensions of 1080 × 1080 km, 144 × 144 km, and 52 × 52 km, respectively. Eighteen vertical sigma layers between the surface and 5000 Pa were used in domains 1 and 2, and 33 vertical sigma layers were used in domain 3.

used in the 36- and 12-km resolution simulations, and 33 vertical sigma layers are used for the 4-km resolution simulation.

[22] To ensure an annual balanced ecosystem CO_2 exchange, we applied the method of *Denning et al.* [1996] to scale microbial, root, and stem respiration. In this approach, the model was first run for the 4-month simulation period (i.e., March, June, September, and December), and the cumulative net ecosystem exchange was computed at each grid point. The 4-month simulation was then performed again, but with microbial, root, and stem respiration scaled by the ratio (R^*) of cumulative G_L (μmol mol m^{-2} s^{-1}) (gross primary production (GPP) minus leaf respiration) to cumulative R (μmol m^{-2} s^{-1}) (sum of microbial, root, and stem respiration),

$$R^* = \frac{\int G_L \mathrm{d}t}{\int R \mathrm{d}t}, \qquad (1)$$

where t is time (s). R^* was calculated separately for each of the three horizontal resolutions. We assumed zero NEE over the ocean at all times and confirmed that the simulations with balanced NEE resulted in no cumulative net CO_2 exchange. While this approach led to relatively realistic NEE estimates over the year, ecosystems may be out of balance with respect to their carbon budget in a particular month. However, this scaling approach guarantees that the net CO_2 fluxes were constrained to be within a realistic range, a condition not generally met by most coupled atmosphere and land-surface models. To test the sensitivity of the recirculation mechanisms described below to our carbon balance approach (equation (1)), we also performed simulations in which NEE was balanced over September alone, instead of across all 4 months. September was chosen for this analysis because it had the largest positive CO_2 anomalies and monthly cumulative NEE.

2.3. Comparing Measured and Predicted CO_2 Concentrations

[23] We compared simulated surface CO_2 anomalies with continuous measurements made by AORG at the Trinidad Head station [*Lueker et al.*, 2001, 2003]. The air samples were drawn every 3 s from a 19-m tall tower at the highest point on Trinidad Head, and analyzed for CO_2 concentration with a modified LICOR model 6251 CO_2 analyzer. CO_2 data were collected and averaged over 4-min intervals.

[24] The measurements needed to be adjusted to make consistent comparisons to the anomalies simulated with the imposed constant boundary conditions in the model. In particular, to compare with the simulated anomalies (ΔCO_2) we required an estimate of the CO_2 background concentration that varied seasonally. We approximated this background CO_2 concentration (C_b (ppm)) as a running previous 7-day average of daily minimum concentrations. The 7-day averaging window was intended to approximate the timescale of typical synoptic events. We tested the impact of this approach by also applying 3- and 11-day lag averages. The standard deviation of the impact of the different lag filters on the predicted background concentration was small (~0.7 ppm) compared to diurnal variations in surface CO_2 concentrations.

[25] In the model versus measurement comparison we used predictions from the Domain 3 grid cell immediately west of Trinidad Head, which is an ocean water surface. We do not expect measurements and model predictions to precisely match since we manipulated the data to estimate ΔCO_2 as described above and we did not prescribe actual CO_2 concentration boundary conditions in the simulations. However, we do expect that synoptic and diurnal patterns in ΔCO_2 during each season will be consistent between the simulations and measurements.

[26] Even at the finest resolution the model does not resolve the Trinidad Head outcrop on which the sampling station is located. It is therefore difficult to know which air parcel was being sampled at the tower. In particular, was the tower sensing the surface layer from over the ocean, or had the airflow diverted around the outcrop and therefore the tower was sensing air from higher up in the marine boundary layer? To test the impact of our predicted samples to this uncertainty, we sampled the model at the surface layer (0–20 m), the layer centered at 70 m, and the layer centered at 110 m (under the wind speed restrictions shown in Table 1). Differences in predicted monthly averaged ΔCO_2 between the 70 m and 110 m sampling heights were small (<0.03 ppm) in June, September, and December and about 0.1 ppm lower at the higher elevation in March.

[27] The largest differences between the surface and 110 m predicted ΔCO_2 were in March and June. In March, monthly averaged ΔCO_2 at 70 m was about 0.1 ppm smaller

Table 1. Wind Speed Sampling Restrictions

Sampling Protocol[a]	u_r, m s^{-1}	v_r, m s^{-1}
S_1	2	4
S_2	3	6
S_3	4	8

[a]Samples are collected in the simulations if the time is between 1000 and 1800 LT and the longitudinal wind speed is greater than u_r and the zonal wind speed is less than v_r.

than at the surface. In June, monthly averaged elevated ΔCO_2 was, counter-intuitively, about 0.2 ppm higher at 110 m than at the surface. Differences between predicted surface and elevated ΔCO_2 were less than 0.05 and 0.01 ppm in September and December, respectively. We therefore conclude that uncertainties associated with uncertainty in sample elevation did not substantially impact predicted ΔCO_2. This conclusion is consistent with the ABL being well mixed during periods when the sampling protocol was met (i.e., during high wind speeds in the middle of the day).

[28] We also compared the monthly mean background CO_2 concentration calculated from the Trinidad Head data with the U.S. National Oceanographic and Atmospheric Administration's (NOAA) estimate of the reference marine boundary layer (MBL) CO_2 concentration [*GLOBALVIEW-CO_2*, 2004]. The GLOBALVIEW-CO_2 concentration estimates are resolved on latitude bands using measurements from active Climate Monitoring and Diagnostics Laboratory sites [*Masarie and Tans*, 1995]. Although the GLOBALVIEW-CO_2 concentrations are broad zonal (along lines of constant latitude) averages of the marine boundary layer, substantial deviations of these values from those measured at Trinidad Head may indicate some influence of local ecosystem CO_2 exchange.

2.4. Sampling Protocol

[29] Atmospheric CO_2 samples used in the global inversions are typically collected during midday and when onshore winds are strong [*Peterson et al.*, 1982, 1986; *Ramonet and Monfray*, 1996; *Haaslaursen et al.*, 1997; *Francey et al.*, 1998]. Flask samples (collected by NOAA) at the Trinidad Head station have typically been taken when winds are larger than 2 m s^{-1}, from the north or northwest, and on Wednesday afternoons (John Miller, personal communication, 2004).

[30] For the model predictions, we chose three sampling protocols (S_1, S_2, and S_3) that each restricted the zonal wind speed, u (m s^{-1}), to be above a certain value (u_r) and the meridional wind speed, v (m s^{-1}), to be below a certain value (v_r), thereby insuring that the winds are predominantly onshore (Table 1). These sampling protocols also restrict sampling times to between 1000 and 1800 local time (LT). Note that S_2 and S_3 are stricter than those currently applied at Trinidad Head. The domain 3 results (4 km resolution) were used in this sampling analysis, with samples taken from the model output every 2 hours. Thus there were five potential samples (at each elevation) from the model predictions each day, and approximately 150 potential samples per month.

3. Results

3.1. Terrestrial Ecosystem NEE and Atmospheric CO_2 Concentrations

[31] Both March and December had relatively balanced predicted monthly NEE across the domain, whereas June was a net CO_2 sink and September was a net CO_2 source (Table 2, column 2). Predicted cumulative NEE are broadly consistent with measurements in Pacific Northwest regrowing forests [e.g., *Law et al.*, 2004], although the source strength in September may be an overestimate. We address the impact of this source strength on predicted ΔCO_2 below.

[32] A consistent pattern of diurnal surface CO_2 concentrations exists at sites inland of Trinidad Head. Figure 2a shows a typical example of predicted ΔCO_2 vertical profiles in mid-September at the grid cell immediately inland from the Trinidad Head station; this grid cell is on the slope leading up toward the coastal mountain range. At 0100 LT, CO_2 concentrations near the surface have increased substantially due to the low stable nocturnal boundary layer and nighttime ecosystem respiration. By 0700 LT the mixed layer elevation has begun to increase and CO_2 concentrations above the earlier nocturnal boundary layer depth have begun to increase as the previous night's respiration is mixed upward. At 1300 LT, net ecosystem uptake has depleted the profile in CO_2 to just above background levels, and ΔCO_2 varies by less than 0.5 ppm within the ABL. By 1900 LT, increases in near-surface ΔCO_2 result from the reduced mixed layer height and the transition to positive net ecosystem CO_2 source. Figure 2b shows predicted surface CO_2 concentration and ABL depth, ending with the day shown in Figure 2a. There is a clear inverse relationship between ΔCO_2 and ABL depth caused by the phasing of NEE and ABL depth.

[33] Note that over flat terrain at continental sites (i.e., in the absence of sea and land breezes and katabatic winds), CO_2 concentrations at night can increase more than 80 ppm above midday values [e.g., *Denning et al.*, 2003] (www.arm.gov, http://co2anal.lbl.gov/worldview/data.html). Interactions between the land and relatively cooler ocean substantially change the ABL dynamics at the coast, and the surface winds associated with the coastal boundary also make the relationship between ABL height and surface CO_2 concentrations more complex. We discuss these complexities and

Table 2. Effect of Sampling Protocol on CO_2 Anomalies at Trinidad Head, California

Month	Mean NEE, gC m^{-2} month^{-1}	Number of Samples Collected			Percent of Samples With Positive ΔCO_2			Average (SD) ΔCO_2, ppm		
		S_1	S_2	S_3	S_1	S_2	S_3	S_1	S_2	S_3
March	−11.2	15	8	3	87	75	67	0.53 (0.73)	0.34 (0.64)	0.57 (0.88)
June	−81.2	32	19	4	59	74	100	0.34 (0.93)	0.29 (0.41)	1.2 (0.75)
September	105.7	44	31	12	80	77	92	3.1 (4.2)	0.86 (1.1)	0.83 (0.53)
December	−13.3	6	7	5	83	71	80	0.05 (0.08)	0.04 (0.12)	0.06 (0.09)

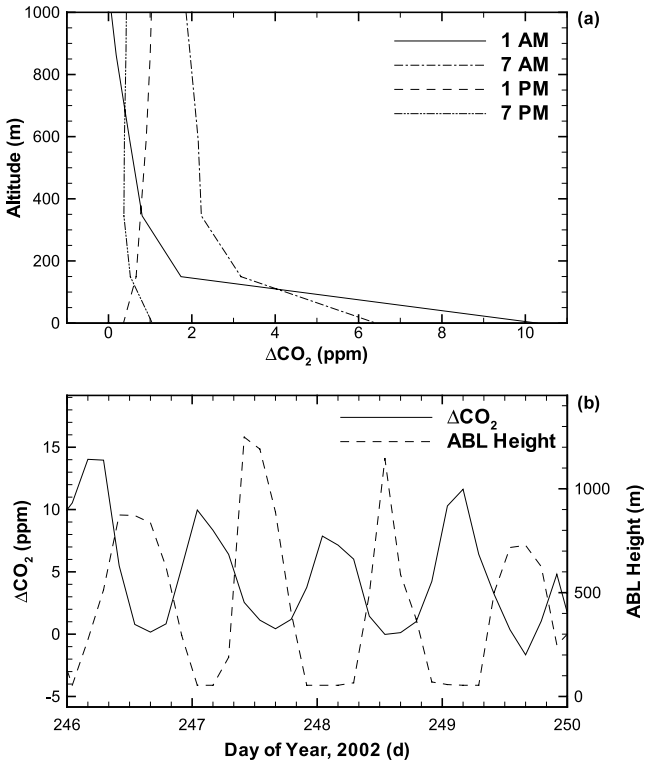

Figure 2. (a) Typical predicted ΔCO_2 profiles within the ABL. These results are from JD 249 and the grid cell immediately inland from the Trinidad Head station (using the domain 2 results). (b) Predicted surface CO_2 concentration and PBL height during September 2002 for the same site as in Figure 2a. For typical inland sites, CO_2 concentration and ABL depth are inversely related. During the night, when the ABL depth is small, respiration increases near-surface CO_2 concentrations substantially. During the day, when the ABL depth is typically large, negative CO_2 anomalies resulting from ecosystem uptake are mixed into this larger volume, and therefore do not impact surface concentrations as strongly. The modeled surface layer extends to about 20 m above the surface.

their impacts on predicted nighttime CO_2 concentrations below.

3.2. Comparing Measured and Predicted CO_2 Concentrations

[34] Generally, the model reasonably predicted diurnal and synoptic variability of the surface CO_2 concentration at Trinidad Head during March, June, September, and December. Figure 3 shows measured (minus C_b, as described above) and predicted ΔCO_2 in the model surface layer. Note that the magnitude of the diurnal and synoptic variations are relatively unaffected by the correction for C_b. The smallest diurnal cycles in measured and predicted surface CO_2 concentrations occurred during March and December. The magnitude of the diurnal cycle depends on both local CO_2 sources and sinks and meteorology, as discussed below.

[35] Although difficult to diagnose, explanations for discrepancies between the measurements and model predictions include incorrect estimates of nighttime respiration, atmospheric transport, nighttime ABL dynamics, and impacts of the imposed constant CO_2 eastern boundary condition. Local marine CO_2 fluxes were also likely reflected in the data, particularly during strong upwelling events known to occur from May to October. The impact of CO_2 fluxes associated with these brief instances of coastal upwelling can produce anomalies of up to 2 ppm at Trinidad Head, and can be identified using simultaneously collected O_2 measurements [*Lueker*, 2004]. Minor upwelling CO_2 fluxes during our study period occurred on days 88–90, 155–160, and 262–266, resulting in estimated CO_2 anomalies of less than 1 ppm at the sampling station. These upwelling events may be partly responsible for the differences between measurements and predictions in September 2002. *Lueker et al.* [2004] found no evidence of significant impacts from urban pollution during our study period, although no trace gases measured at Trinidad Head by the AGAGE program can quantitatively confirm this. Future work will use the continuous O_2 record to identify periods when fossil fuel CO_2 emissions are impacting the sampling station. However, given the location of the Trinidad Head Station, we contend that fluxes from the adjacent forests and ocean constitute the main features seen in the CO_2 record.

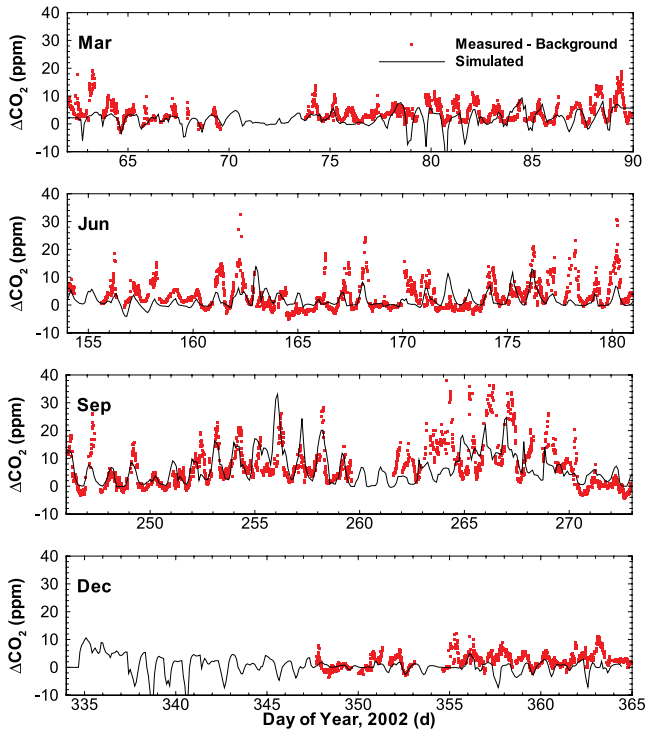

Figure 3. Comparison between simulated and measured CO_2 concentrations at Trinidad Head, California, for March, June, September, and December 2002. Note that we do not expect measurements and models to precisely match since we do not prescribe realistic CO_2 concentration boundary conditions. Fossil fuel or marine upwelling CO_2 fluxes could also be impacting the comparison. An estimated background CO_2 concentration (calculated as a running 7-day average of daily minimum concentration) is subtracted from the data so that comparisons can be made to the simulations, and the first 3 days of each month are excluded to allow for model spin-up.

[36] The model simulated ΔCO_2 concentrations during March reasonably well, although nighttime peak ΔCO_2 values were underestimated by a few ppm about half of the days. The substantial reductions in predicted ΔCO_2 around JD 80 were not reflected in the data. On these days the model predicted recirculation of a negative CO_2 anomaly that was not observed at Trinidad Head. This 4-day period and 7 days during December (where no data were available for comparison during five of those days) were the only times during the 4 months where this type of strong negative anomaly was predicted. Although the data covered only about half the month of December, the model generally captured the daytime ΔCO_2 minima, but underestimated nighttime peak ΔCO_2 values.

[37] During June the model predicted the minima and phasing of ΔCO_2 values, but underpredicted nighttime peak ΔCO_2 values for about half of the nights. On days 177 to 181, modeled ΔCO_2 concentrations was substantially lower than observations. During this period, measured winds from a nearby airport were from the south to southeast while the model predicted winds from the north to northwest with very little diurnal variability. As discussed below, this discrepancy is consistent with the relationship between nighttime katabatic flows, nighttime respiration, and measured CO_2 concentrations at the station.

[38] During the first 2 weeks of September the model successfully simulated ΔCO_2 values in phasing, daytime minima, and nighttime maxima. On days 255–260 both the model and measurements suggest large diurnal variations in NEE, and elevated surface CO_2 concentrations during periods of onshore winds. These positive ΔCO_2 values resulted from a combination of nighttime respiration and nighttime offshore winds followed by strong onshore winds during the next afternoon. We use this period below to investigate the impact on measured surface CO_2 concentrations of respired CO_2 that has circulated out to sea during the night and returned to the coast during the day. A similar phenomenon occurred on days 264–269 where the measurements and model showed elevated nighttime and daytime ΔCO_2 values, as compared with the background. Although the model also predicted these features, it underestimated the nighttime peaks and overestimated daytime minima for several of the days. We believe this period also illustrates large-scale recirculation of respired CO_2. Upwelling events may also be responsible for a small portion of these differences between measurements and predictions.

[39] As mentioned above, the large diurnal cycles in measured CO_2 concentration at the sampling station do not, in themselves, imply that midday CO_2 samples are impacted by local terrestrial ecosystems. The next section presents predicted anomalies for samples collected during periods that have previously been assumed to represent clean marine boundary layer air: onshore wind conditions during midday. We then describe the mechanisms influencing the predicted positive and negative CO_2 anomalies at the sampling station.

3.3. Impact of Sampling Protocol

[40] Only a fraction of the approximately 150 possible monthly samples met the individual sampling protocols (Table 2, columns 3–5). For example, about 10, 20, 30, and 4% of the potential samples met the S_1 sampling

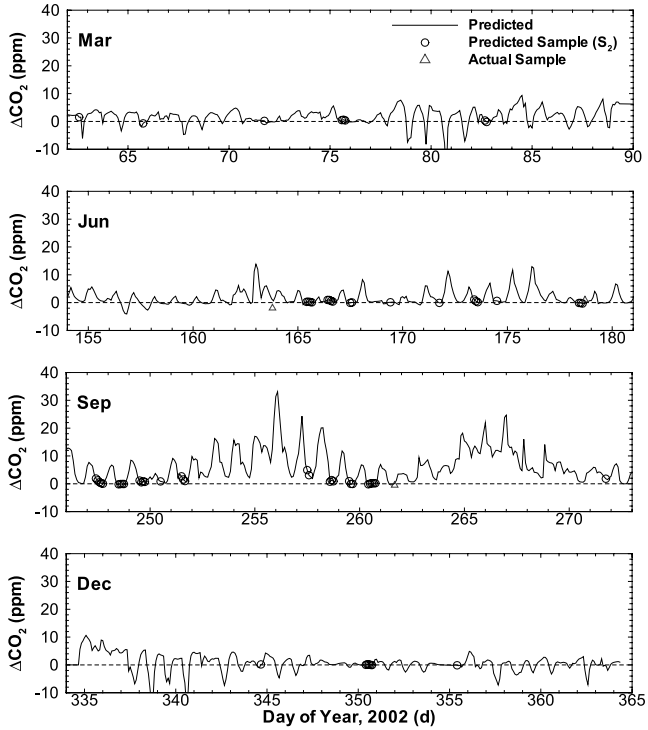

Figure 4. Predicted ΔCO_2, predicted samples under sampling protocol S_2, and actual flask samples. A 7-day average minimum CO_2 concentration (from the continuous measurements) has been subtracted from the flask sample measurements as in Figure 3.

protocol in March, June, September, and December, respectively. All three sampling protocols led to positive and negative predicted ΔCO_2 values during individual months. However, of the samples taken, the large majority had positive ΔCO_2 anomalies during all months and for all sampling protocols (Table 2, columns 6–8). For example, Figure 4 shows the times that samples met the S_2 protocol during each month. All of the monthly averaged ΔCO_2 values (that met the criteria for each of the three sampling protocols) were positive (Table 2, columns 9–11), implying that the CO_2 signal associated with nighttime respiration sources was more likely to be sampled than the daytime CO_2 sinks. For example, with the S_1 protocol, monthly average ΔCO_2 values were 0.53 ± 0.73 ppm, 0.34 ± 0.93 ppm, 3.1 ± 4.2 ppm, and 0.05 ± 0.08 ppm for March, June, September, and December, respectively. Note that the standard deviations were relatively large because predicted ΔCO_2 during the sampling intervals included negative values. The high positive ΔCO_2 in September occured because six samples were predicted to be taken between JD 264 and 267, a period with very high midday ΔCO_2 values (discussed below).

[41] As the sampling protocol becomes more restrictive (i.e., between S_2 and S_3), the ΔCO_2 monthly average in March and June, counter-intuitively, increased substantially (a small increase also occurred in December). This feature partially resulted from the greater uncertainty associated with reduced sample size. Only three and four samples satisfied the most stringent sampling protocol (S_3) during

March and June, respectively. For June, the increase in model ΔCO_2 samples was caused by increasing v_r to 8 m s^{-1}, which allowed several points with large alongshore flow components into the average that were not included in the S_2 samples. However, the small number of samples implies that the predicted anomalies may not be robust for the S_3 protocol.

[42] The size of the positive monthly ΔCO_2 was only weakly connected with the size of the monthly mean NEE (Table 2, column 2), although September had high values of both NEE and ΔCO_2. For example, June had a high monthly averaged ΔCO_2 (under sampling protocol S_3) even with strong negative monthly NEE. To test the sensitivity of our September ΔCO_2 predictions to the predicted positive monthly mean NEE, we performed another simulation where equation (1) was used to balance NEE in September alone. The monthly ΔCO_2 values obtained using the S_1, S_2, and S_3 protocols decreased to 1.4, 0.41, and 0.40 ppm, respectively. Although smaller than anomalies predicted when NEE across all 4 months was balanced, the positive values under conditions of zero net monthly NEE indicate that recirculation of nighttime respired CO_2 was prevalent in September.

[43] The anomalies, both positive and negative, simulated at the sampling station resulted from transport of CO_2 anomalies recently generated by local terrestrial ecosystems (hereinafter referred to as ''recirculation''). An important feature of the monthly averaged CO_2 concentrations predicted at the coastal station is their consistent positive bias with respect to background values. Two closely related mechanisms generated the positive CO_2 recirculation. First, if there are broadly offshore winds during the night and onshore winds during the day, then CO_2 produced at night and transported out over the ocean can come back ashore at about the same latitude during the next day. For Trinidad Head, the offshore winds are often katabatic, i.e., are generated from pressure gradients associated with radiative losses from coastal mountain slopes. Second, larger spatial scale mixing can result from a combination of offshore, alongshore, and onshore flows. For example, respired CO_2 produced in Oregon can be transported out over the ocean during the night and transported south (for a period of several days) before being flushed ashore at the Trinidad Head sampling station.

[44] The simulations also predicted instances of daytime CO_2 uptake anomalies being mixed into the ABL, transported offshore during the night, and returned to the coast during the next day. All months had some predicted negative anomalies, and June and September had many under sampling protocols S_1 and S_2.

[45] Characterizing the recirculation mechanisms that led to non-zero ΔCO_2 at the sampling station requires an understanding of the large-scale and local wind fields on hourly timescales. The next section describes measurements and model predictions of these fields.

3.4. Wind Direction

[46] Large-scale winds interact with the coastal boundary, local topography, and flows generated near the surface (e.g., katabatic winds) to generate local winds that are often quite different from the large-scale flow. Figure 5 shows the predicted wind direction at the surface in the grid cell immediately west of Trinidad Head (from the domain 3 simulation; representative of local winds) and in the grid cell at 10 km elevation directly above Trinidad Head (from the domain 1 simulation; representative of the large-scale flow in the free troposphere). Also shown are measurements from the Eureka Arcata Airport, which is on the coast about 16 km south of Trinidad Head. Unfortunately, a meteorological station was not installed at the Trinidad Head station until after the period of this study.

[47] Wind direction changes on diurnal, synoptic, and seasonal timescales. We compared the measured and predicted diurnal wind direction patterns by calculating the difference between nighttime (0000 to 0400 LT) and daytime (1200 to 1600 LT) average wind directions. We chose this comparison because this diurnal variability in wind direction is critical for explaining terrestrial ecosystem impacts on CO_2 samples at the station. Over the 4 months simulated, the predicted differences in nighttime versus daytime wind direction were within 22.5° and 10° of measured differences 86% and 83% of the time, respectively. Further, the predicted weekly and seasonal surface wind direction variability at Trinidad Head generally agrees well with the measurements from the airport. We therefore conclude that the predicted variations in wind direction were sufficiently accurate to characterize the coupling between transport and ecosystem exchanges described below.

[48] Predicted local surface wind directions at Trinidad Head showed more diurnal variability than the large-scale flow (sampled at 10 km height). In March, the model predicted that about half the days had local wind directions from the south to west. The remainder of the month had several multiday periods with diurnal reversals in wind direction that are consistent with the measurements. For a large portion of June, the predicted local wind directions were more consistent, typically being from the northeast at night and from the north during the day; this diurnal variability was also present in the measurements but absent in the predicted large-scale flow in the free troposphere. The measurements during June also show more local-scale variability in wind direction than the model predicted for about a third of the month. During September, there were large diurnal swings in wind direction (again present in the surface measurements and model predictions, but absent from the predicted large-scale wind fields), generally from the east to southeast at night and from the west to northwest at midday. Note that September also had the largest monthly averaged ΔCO_2. Finally, in December, the predicted and measured local wind directions varied diurnally in the first week and showed little diurnal variability for the rest of the month, originating generally from the southwest.

3.5. Recirculation of Respired CO_2

[49] The period in September (i.e., days 252–260) where positive anomalies (Figure 4) and diurnal onshore and offshore winds (Figure 5) occurred illustrates the recirculation of CO_2 respired the previous night. During the evening, near-surface CO_2 concentrations were elevated owing to ecosystem respiration and the low stable nocturnal boundary layer. Figure 6 shows the September average modeled diurnal ABL depth on a zonal transect through Trinidad Head. Relatively constant sensible heat fluxes lead to a relatively constant ABL depth over the ocean. The ABL

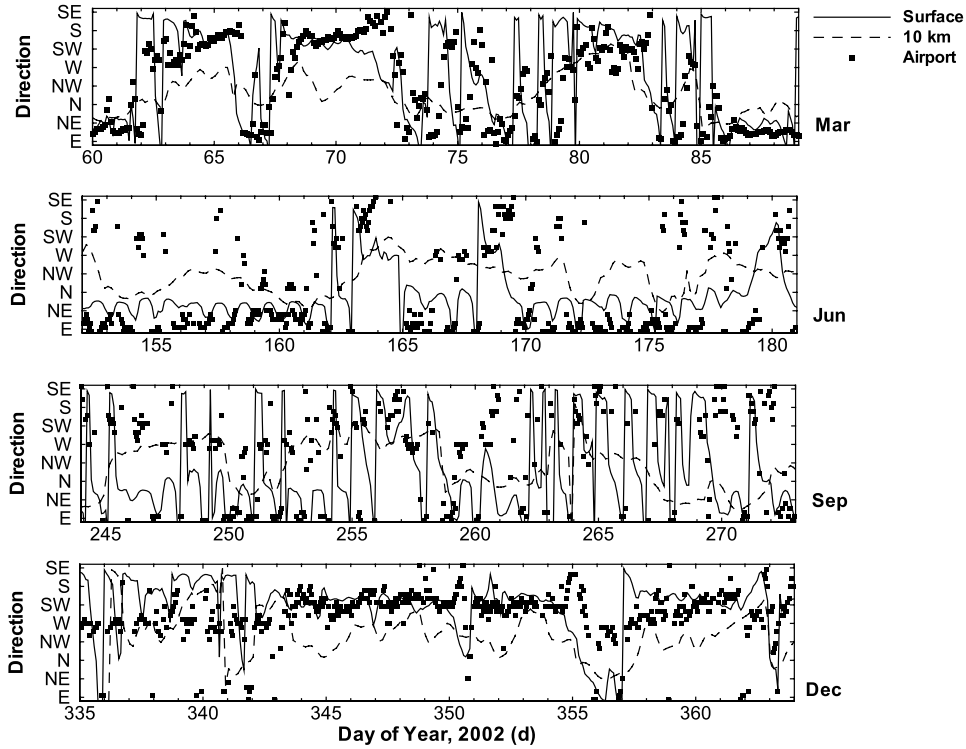

Figure 5. Predicted surface (solid lines) and 10-km elevation (dashed lines) wind direction at Trinidad Head for the 4 months. Also shown are measurements from the Eureka Arcata Airport, which is on the coast about 16 km south of Trinidad Head. The model broadly matches measured diurnal and seasonal wind direction variability. Diurnal wind direction changes are much more variable near the surface than aloft. The difference between surface and synoptic-scale wind direction was most pronounced during September.

depth over land increases during the day from increased convective motion driven by the warming of the land surface.

[50] Predicted surface ΔCO_2 and wind vectors for the Domain 3 simulation on JD 258 are shown in Figure 7. Strong offshore katabatic winds were present at midnight, with a convergence zone about 10 km offshore. The large positive ΔCO_2 generated over land (~25 ppm) was advected offshore with these winds. At 0200 LT, the anomaly was reduced from this high level at the coast to about 5 ppm toward the western end of the domain owing to mixing into the relatively higher ABL depth over the ocean. Between 0200 and 1000 LT the surface winds rotated until they were from the south to southwest. At 1000 LT the winds had an onshore component and carried a ΔCO_2 of 5 to 10 ppm. By noon the surface winds were directly onshore and a several ppm positive ΔCO_2 was blown back across the sampling station. Finally, by 1600 LT, ΔCO_2 was effectively zero, and background air was being sampled at the station. The large negative ΔCO_2 generated by ecosystem uptake inland of the station was mixed into the high ABL depth over land and transported toward the east. By 2000 LT, ecosystem respiration was again increasing ΔCO_2 near the surface. The westward katabatic flow was not strong enough to oppose the prevailing onshore wind until around midnight (not shown), as in the previous evening.

[51] Larger spatial scale mixing of respired CO_2 also impacted ΔCO_2 measured at the Trinidad Head station. For example, during the period JD 264–268, both simulations

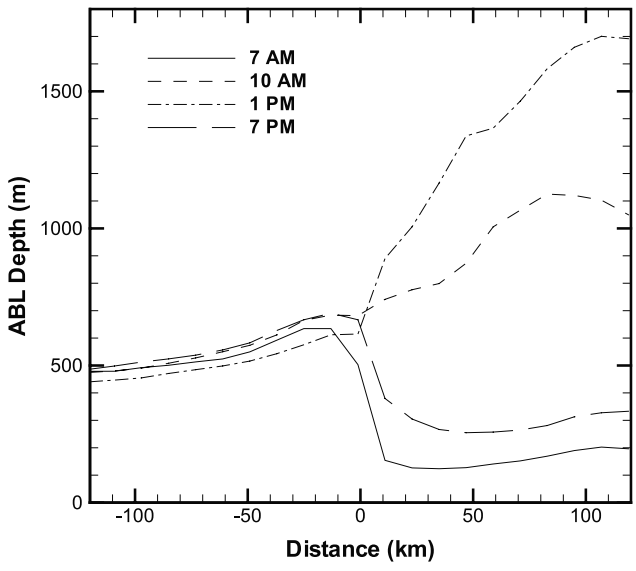

Figure 6. September monthly averaged ABL depth versus distance from the coast at the Trinidad Head latitude (positive distance indicates eastward) for several times of day. Typically, the ABL depth over land during the night is low and over the ocean is relatively higher. As the land warms in the morning, the ABL depth over land increases due to the resulting buoyant convection.

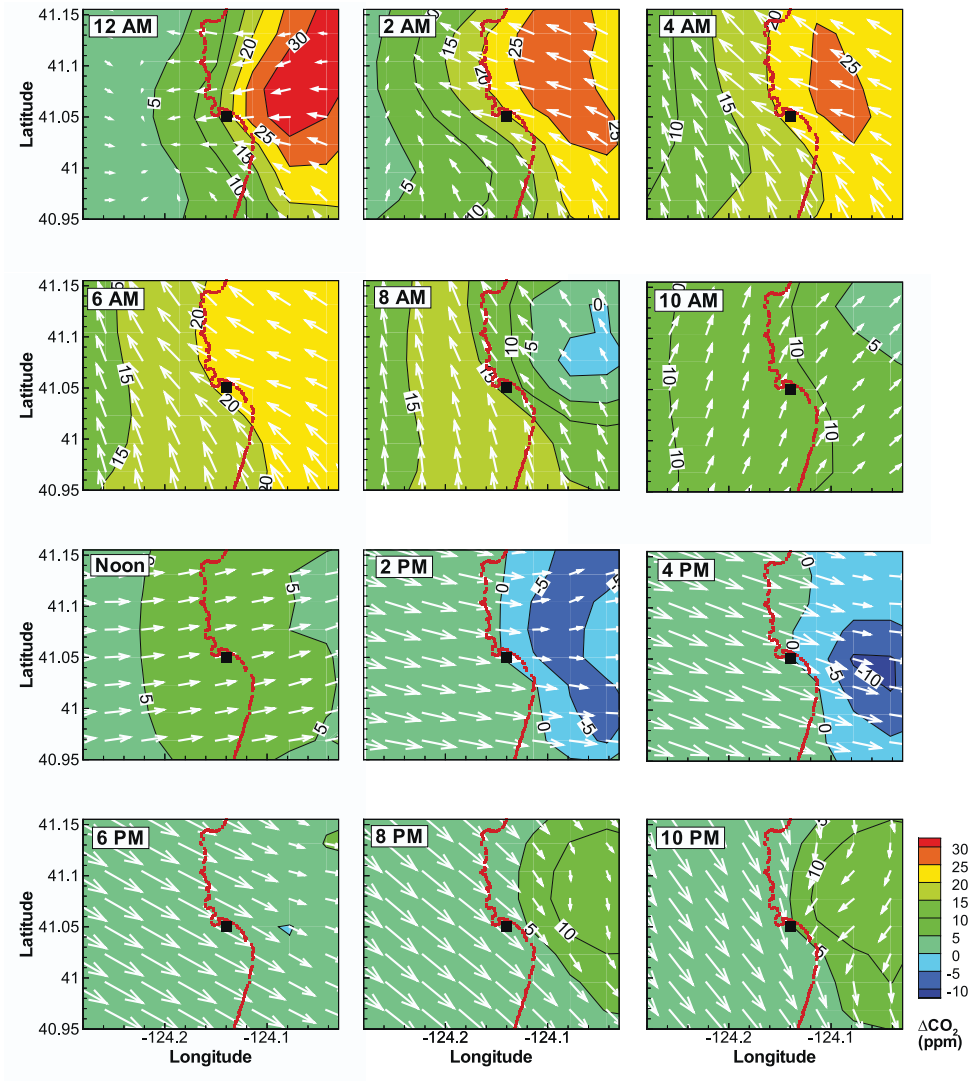

Figure 7. Surface ΔCO_2 contours and horizontal wind vectors on JD 258. Offshore winds during the night drive elevated CO_2 concentrations out to sea. As the winds shift to onshore in the morning this positive anomaly in CO_2 concentration is recirculated back over the sampling station (indicated by the black square). The red line indicates the coastline.

and measurements showed positive ΔCO_2 (Figure 3). In addition to the mechanisms described above, there also is substantial north to south transport of positive ΔCO_2 during this period. Figure 8 shows predictions (domain 1) of surface ΔCO_2 and horizontal wind vectors for one day during this period (JD 266). Positive ΔCO_2 as high as 25 ppm created in the northern portion of the simulated domain were advected out over the ocean by katabatic winds, as described above. Again, this signal was diluted as it mixes into the higher ABL depth over the ocean, although peak ΔCO_2 levels remain relatively high (up to 15 ppm). In this case, though, large-scale winds transported the positive anomaly southward. By 1000 LT, the positive anomaly extended ~100 km offshore, and by 1300 LT, onshore winds near the coast were drawing the anomaly over the Trinidad Head station. At 1900 LT the anomaly was still moving over the station and southward. Although this example is an extreme case shown to illustrate the mechanism, alongshore transport of positive anomalies associated with nighttime offshore flow occurs regularly during periods of high ecosystem respiration.

[52] Terrestrial CO_2 exchanges impacted surface ΔCO_2 farther than 100 km offshore from Trinidad Head (Figure 9 shows results for September). The difference in ΔCO_2 between the coast and over the ocean varied the least in March and December, and the most in June. For all months, there were periods with substantial diurnal cycles in predicted surface ΔCO_2 100 km from shore. The daytime reduction in predicted offshore ΔCO_2 did not result from enhanced terrestrial uptake and transport, but rather from mixing with background air that was moving eastward over the ocean. In contrast, the nighttime increases in offshore ΔCO_2 were a result of positive NEE during the night and offshore winds.

3.6. Recirculation of Daytime CO_2-Depleted Air

[53] During the day, ecosystem CO_2 uptake establishes a negative ΔCO_2 in the well-mixed layer below the ABL.

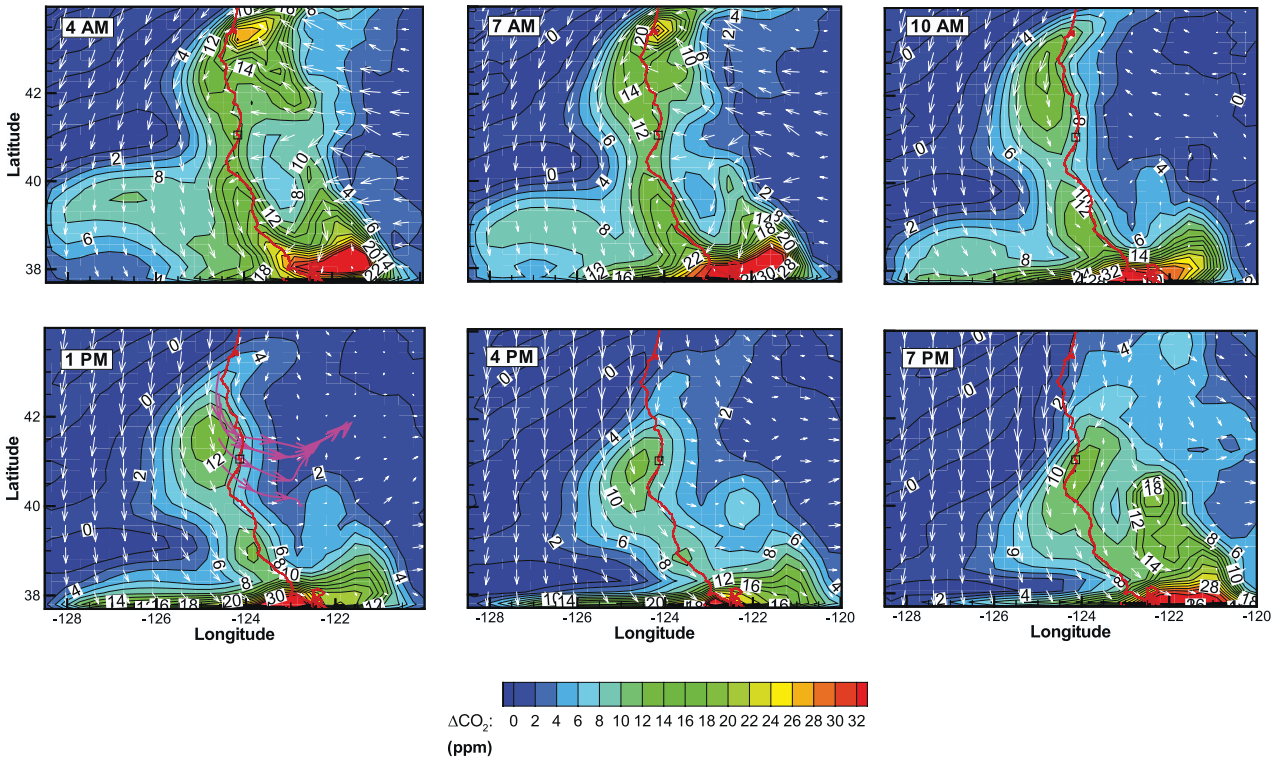

Figure 8. Surface ΔCO_2 contours and horizontal wind vectors for 6 times on JD 266. This period illustrates large-scale recirculation of CO_2 produced during nighttime ecosystem respiration. Streamlines (purple) are shown at 1300 LT to illustrate transport of positive ΔCO_2 onshore in the middle of the day (the actual streamlines will differ since the velocity field changes over time). The Trinidad Head station is indicated by the black square in the center of the figure, and the red line indicates the coastline.

After sunset, a residual layer typically establishes above the low nighttime ABL and below a capping inversion [*Stull*, 1988]. Negative ΔCO_2 values resulting from the previous day's ecosystem uptake are preserved, to some extent, in this residual layer. If an elevated nighttime offshore breeze exists, this negative ΔCO_2 can be transported offshore, entrained in the marine boundary layer, and transported back over the coast. This phenomenon is fundamentally three-dimensional; that is, in addition to zonal and vertical transport, there is substantial meridional (along lines of constant longitude) CO_2 transport. However, examining a cross section through the Trinidad Head station latitude illustrates the processes responsible for the negative ΔCO_2 simulated at the station.

[54] An example of the impact of these mechanisms is shown in Figure 10 for JD 166. A small contour range has been applied to emphasize the relatively small ΔCO_2 values, so that the figure does not distinguish ΔCO_2 values less than -0.5 or greater than 0.5 ppm. By 0100 LT on JD 166, a low ($\sim$100 m) stable nocturnal boundary layer has developed, ecosystem respiration has increased ΔCO_2 near the surface, and the negative ΔCO_2 formed the previous daylight period was preserved in the residual layer. Qualitatively, these features are similar to results from the two- and three-dimensional simulations of *Lu and Turco* [1994, 1995]. At 0100 LT, there was onshore flow over the ocean below $\sim$500 m altitude, and an offshore flow above the residual ABL over the land; the flows converged near the coastline.

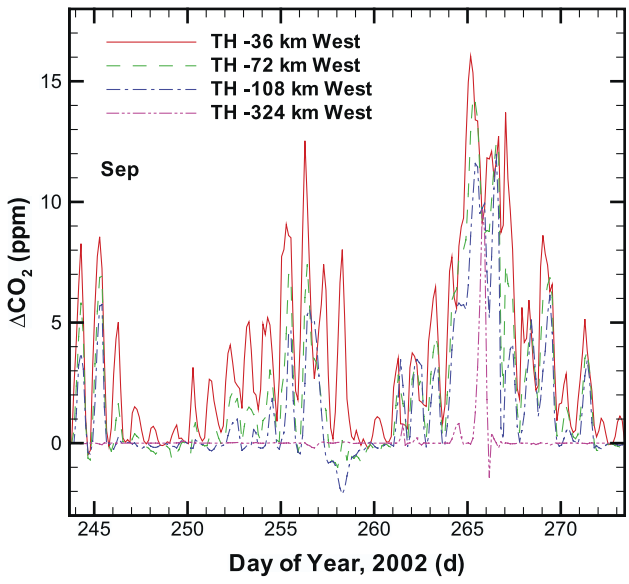

Figure 9. Predicted offshore surface ΔCO_2 in September 2002. During September, nighttime offshore breezes transported significant amounts of respired CO_2 out greater than 100 km over the ocean. The grid point 324 km offshore from the Trinidad Head station was typically unaffected by terrestrial CO_2 exchanges, except during the strong offshore transport around JD 265.

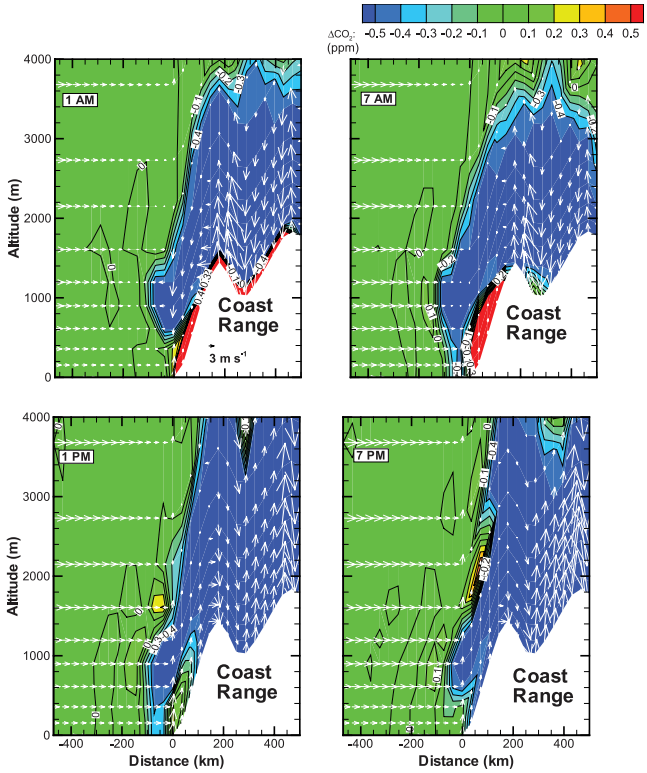

Figure 10. Vertical ΔCO_2 contours and wind vectors on JD 166. The terrain is shown as solid white, the vertical velocity has been scaled by a factor of 30, and the contour range has been decreased to illustrate small perturbations in ΔCO_2. Midday negative ΔCO_2 values directly offshore occur because the negative ΔCO_2 generated the previous day was preserved in an elevated residual layer, transported offshore, and entrained in the marine boundary layer.

By 0700 LT the negative ΔCO_2 has been entrained into the marine boundary layer. In contrast to other periods, the low-level onshore winds were strong enough over this night to oppose katabatic transport of the positive ΔCO_2 generated from ecosystem respiration out over the ocean. The winds were predominantly onshore by 1300 LT, and the negative ΔCO_2 was advected toward the sampling station at the coast. By 1900 LT the negative ΔCO_2 had swept past the sampling station. On this day, using sampling protocol S_1, the simulations predicted that ΔCO_2 samples of -0.22 and -0.08 ppm would have been measured at 1000 and 1200 LT, respectively.

3.7. Background CO_2 Concentration From Measurements

[55] Continuous (C_b) and monthly mean ($\overline{C}_b$) seven-day lag averages of the minimum daily CO_2 concentration measured at Trinidad Head are shown in Figure 11. Note that there were insufficient data to form monthly averages in February and November. Also shown are monthly mean marine boundary layer background CO_2 estimates from the GLOBALVIEW-CO_2 database for the two zonal bands surrounding Trinidad Head. If air sampled at Trinidad Head was representative of background marine boundary layer air, we expect C_b to fall roughly between the two GLOBALVIEW-CO_2 concentration estimates.

[56] Differences between the GLOBALVIEW-CO_2 estimates of marine boundary layer CO_2 concentrations and $\overline{C}_b$ follows a clear pattern. Between December and May, $\overline{C}_b$ fell roughly within the GLOBALVIEW-CO_2 bounds (excepting January). June and July monthly averages were close to those from the more northern GLOBALVIEW-CO_2 zone. The large temporal variability in continuous C_b between July and November likely reflected terrestrial ecosystem influences. The August $\overline{C}_b$ value was substantially lower than estimates from GLOBALVIEW-CO_2. This difference occured when ecosystems in this region are likely substantial net atmospheric CO_2 sinks [*Falge et al.*, 2002]. September and October $\overline{C}_b$ values were larger than those from GLOBALVIEW-CO_2 and may partly reflect the recirculation of nighttime respired fluxes. Although not a rigorous test, the comparisons shown in Figure 11 are consistent with the hypothesis that local CO_2 sources and sinks are impacting marine background CO_2 concentration estimates at this coastal sampling station.

4. Discussion

[57] Local and large-scale recirculation of nighttime positive ΔCO_2 from ecosystem respiration and recirculation of negative ΔCO_2 resulting from daytime net ecosystem uptake suggest that, even with strict wind speed and direction sampling protocols, it may be impossible to exclude the effects of the local terrestrial biosphere on coastal CO_2 observations. In contrast to what might

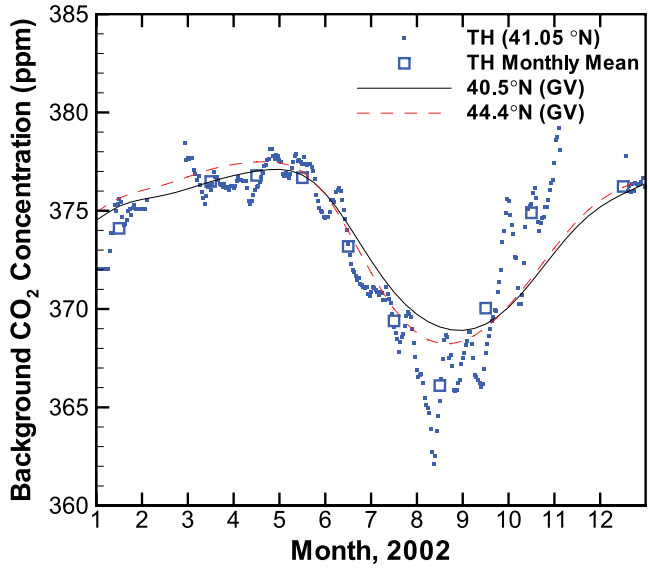

Figure 11. GLOBALVIEW-CO_2 marine background CO_2 concentrations (GV) for two zonal bands surrounding the sampling station and continuous and monthly averaged background CO_2 concentrations estimated from measurements at Trinidad Head. Large differences between GLOBALVIEW-CO_2 and measured values indicate periods when local ecosystem NEE may be impacting marine background CO_2 estimates. No CO_2 data were collected in February and November.

be inferred from continental interior measurements and analyses, in the middle of the day at Trinidad Head it was more likely that the terrestrial biosphere contributes to a positive CO_2 anomaly than a negative one. Further, our predicted positive monthly CO_2 anomalies are likely to be conservative estimates because many nights we underestimated the peak surface CO_2 concentrations at Trinidad Head (Figure 3).

[58] Tracers have been used at other coastal and island sampling sites to exclude periods where local terrestrial ecosystem exchanges can bias sample interpretation. For example, ^{222}Rn [*Whittlestone et al.*, 1992] and ^{212}Pb [*Whittlestone et al.*, 1996] have been proposed as tracers at the Mauna Loa Observatory and ^{222}Rn and CO have been used at Cape Point [*Brunke et al.*, 2004]. Notably, *Brunke et al.* [2004] reported that wind speed selection at Cape Point was of no value for discerning whether sampled air had recently been impacted by local sources. Similar measurements, particularly ^{222}Rn, could help isolate periods at Trinidad Head when samples are comprised predominantly of "clean" marine layer air.

[59] The magnitude of the anomalies predicted here suggests a substantial impact on regional and global CO_2 inversions that do not resolve local circulations. For example, averaged over the year with the S_1 protocol, we predict the local terrestrial biosphere would lead to CO_2 anomalies at Trinidad Head of $\sim$1 ppm. This offset is substantial given that CO_2 gradients reported across North America are often less than 1 ppm [*Fan et al.*, 1998] and that an interhemispheric difference in surface concentration of 0.8 ppm between 45°N and 45°S corresponds to a 1 Pg C Northern Hemisphere carbon sink [*Olsen and Randerson*, 2004]. Global models (that did not resolve katabatic flows and air-sea circulations) would overestimate the size of a North American carbon sink if the recirculation processes described above were stronger at observation sites on the west coast (e.g., Point Reyes, California, Trinidad Head, California, and Cape Meares, Oregon) than on the east coast (e.g., Bermuda East, Bermuda West, or Key West, Florida). We expect that impacts of recirculation on the east coast of the United States will be quite different from the effects described here, since coastal mountains are smaller and winds are predominantly offshore (and weaker) for much of the year. We intend to quantify recirculation effects at other coastal and island stations in future work, as well as quantifying the effect of coastal meteorology and mixing on vertical CO_2 gradients established from remote sources and sinks.

5. Conclusions

[60] Terrestrial CO_2 exchanges and complex coastal meteorology can affect sampling at the coast, even during midday conditions with strong onshore winds. Predicted monthly averaged CO_2 anomalies at the sampling station, which were all positive, were not well correlated with monthly NEE. We identified two classes of coupled surface flux and transport mechanisms that impact CO_2 samples collected at the coast. First, and most important, is local and large-scale recirculation of nighttime positive ΔCO_2 from ecosystem respiratory fluxes being entrained into katabatic flows off the coastal mountain range. This mechanism leads to positive CO_2 anomalies in samples collected under conditions designed to ensure that the onshore flow represents "background" marine boundary layer air. The second class of mechanisms is recirculation of negative ΔCO_2 resulting from daytime net ecosystem uptake. The nighttime residual layer of negative ΔCO_2 can be transported offshore and then entrained in the eastward flowing MBL.

[61] Although our results, interpretations, and conclusions are based on measurements and simulations at Trinidad Head, we believe that the mechanisms described here are prevalent in many coastal flask sampling stations. The magnitude of the predicted effects suggests that these processes influence regional and global CO_2 source and sink inversions. Further work should be conducted to characterize these impacts, determine the extent to which they apply across the flask sampling network (including islands), and develop methods to correct regional and global inversion models that cannot resolve these processes.

Notation

C_b	estimated background CO_2 concentration, ppm.
$\overline{C_b}$	monthly averaged C_b, ppm.
ΔCO_2	CO_2 anomaly; i.e., difference in CO_2 concentration from background, ppm.
G_L	gross primary production minus leaf respiration, μmol m^{-2} s^{-1}.
R	sum of microbial, root, and stem respiration, μmol m^{-2} s^{-1}.
R^*	respiration scale factor.
t	time, s.
u	zonal wind speed, m s^{-1}.
u_r	minimum zonal wind speed, m s^{-1}.
v	meridional wind speed, m s^{-1}.
v_r	minimum meridional wind speed, m s^{-1}.

[62] **Acknowledgments.** We thank Larry Oolman for the wind direction data from the Eureka Arcata airport, David Fitzjarrald for a very helpful review, and Sebastien Biraud for helpful conversations. We also thank NOAA for the GLOBALVIEW-CO_2 estimates of the marine reference background CO_2 concentrations. This work was supported by NOAA Office of Global Programs Award NA03OAR4310059.

References

Banta, R. M., et al. (1997), Nocturnal cleansing flows in a tributary valley, *Atmos. Environ.*, *31*, 2147–2162.

Betts, A. K., and J. H. Ball (1998), FIFE surface climate and site-average dataset 1987–89, *J. Atmos. Sci.*, *55*(7), 1091–1108.

Blumenthal, D. L., W. H. White, and T. B. Smith (1978), Anatomy of a Los Angeles smog episode: Pollutant transport in the daytime sea breeze regime, *Atmos. Environ.*, *12*, 893–907.

Bonan, G. B. (1996), A land surface model (LSM version 1.0) for ecological, hydrological, and atmospheric studies: Technical description and user's guide, *NCAR Tech. Note NCAR/TN-417+STR*, 150 pp., Natl. Cent. for Atmos. Res., Boulder, Colo.

Bonan, G. B., F. S. Chapin III, and S. L. Thompson (1995), Boreal forest and tundra ecosystems as components of the climate system, *Clim. Change*, *29*, 145–168.

Bonan, G. B., K. J. Davis, D. Baldocchi, D. Fitzgerald, and H. Neumann (1997), Comparison of the NCAR LSM I land surface model with BOREAS aspen and jack pine tower fluxes, *J. Geophys. Res.*, *102*(C12), 29,065–29,076.

Brunke, E. G., C. Labuschagne, B. Parker, H. E. Scheel, and S. Whittlestone (2004), Baseline air mass selection at Cape Point, South Africa: Application of Rn-222 and other filter criteria to CO_2, *Atmos. Environ.*, *38*, 5693–5702.

Chen, F., and J. Dudhia (2001a), Coupling an advanced land surface-hydrology model with the Penn State-NCAR MM5 modeling system:

Part I. Model implementation and sensitivity, *Mon. Weather Rev.*, *129*(4), 569–585.

Chen, F., and J. Dudhia (2001b), Coupling an advanced land surface-hydrology model with the Penn State-NCAR MM5 modeling system: Part II. Preliminary model validation, *Mon. Weather Rev.*, *129*(4), 587–604.

Chou, W. W., S. C. Wofsy, R. C. Harriss, J. C. Lin, C. Gerbig, and G. W. Sachse (2002), Net fluxes of CO_2 in Amazonia derived from aircraft observations, *J. Geophys. Res.*, *107*(D22), 4614, doi:10.1029/2001JD001295.

Conway, T. J., P. P. Tans, L. S. Waterman, and K. W. Thoning (1994), Evidence for interannual variability of the carbon cycle from the National Oceanic and Atmospheric Administration Climate Monitoring and Diagnostics Laboratory Global Air Sampling Network, *J. Geophys. Res.*, *99*(D11), 22,831–22,855.

Cooley, H. S., W. J. Riley, M. S. Torn, and Y. He (2005), Impact of agricultural practice on regional climate in a coupled land surface mesoscale model, *J. Geophys. Res.*, *110*, D03113, doi:10.1029/2004JD005160.

Denning, A. S., G. J. Collatz, C. G. Zhang, D. A. Randall, J. A. Berry, P. J. Sellers, G. D. Colello, and D. A. Dazlich (1996), Simulations of terrestrial carbon metabolism and atmospheric CO_2 in a general circulation model: 1. Surface carbon fluxes, *Tellus, Ser. B*, *48*(4), 521–542.

Denning, A. S., M. Nicholls, L. Prihodko, I. Baker, P. L. Vidale, K. Davis, and P. Bakwin (2003), Simulated variations in atmospheric CO_2 over a Wisconsin forest using a coupled ecosystem-atmosphere model, *Global Change Biol.*, *9*(9), 1241–1250.

Dickinson, R. E., A. Henderson-Sellers, P. J. Kennedy, and M. F. Wilson (1986), Biosphere/atmosphere transfer scheme (BATS) for the NCAR community climate model, *NCAR Tech. Note TN275*, 69 pp., Natl. Cent. for Atmos. Res., Boulder, Colo.

Edinger, J. G. (1973), Vertical distribution of photochemical smog in Los Angeles basin, *Environ. Sci. Technol.*, *7*, 247–252.

Edinger, J. G., M. H. McCutchan, P. R. Miller, B. C. Ryan, M. J. Schroeder, and J. V. Behar (1972), Penetration and duration of oxidant air pollution in the south coast air basin of California, *J. Air Pollut. Control Assoc.*, *22*, 882–886.

Falge, E., et al. (2002), Seasonality of ecosystem respiration and gross primary production as derived from FLUXNET measurements, *Agric. For. Meteorol.*, *113*(1–4), 53–74.

Fan, S., M. Gloor, J. Mahlman, S. Pacala, J. Sarmiento, T. Takahashi, and P. Tans (1998), A large terrestrial carbon sink in North America implied by atmospheric and oceanic carbon dioxide data and models, *Science*, *282*, 442–446.

Fischer, M. L., W. J. Riley, and S. Tonse (2004), Development of an implementation plan for atmospheric carbon monitoring in California, *Pap. LBNL-57485*, 38 pp., Calif. Energy Comm., Sacramento, Calif.

Fitzjarrald, D. R. (1986), Slope winds in Veracruz, *J. Clim. Appl. Meteorol.*, *25*(2), 133–144.

Francey, R. J., et al. (1998), Atmospheric carbon dioxide and its stable isotope ratios, methane, carbon monoxide, nitrous oxide and hydrogen from Shetland Isles, *Atmos. Environ.*, *32*, 3331–3338.

Gerbig, C., J. C. Lin, S. C. Wofsy, B. C. Daube, A. E. Andrews, B. B. Stephens, P. S. Bakwin, and C. A. Grainger (2003), Toward constraining regional-scale fluxes of CO_2 with atmospheric observations over a continent: 1. Observed spatial variability from airborne platforms, *J. Geophys. Res.*, *108*(D24), 4756, doi:10.1029/2002JD003018.

GLOBALVIEW-CO_2 (2004), *Cooperative Atmospheric Data Integration Project: Carbon Dioxide* [CD-ROM], Natl. Oceanic and Atmos. Admin./Clim. Monit. and Diag. Lab., Boulder, Colo. (Available via anonymous FTP to ftp.cmdl.noaa.gov, Path: ccg/co2/GLOBALVIEW)

Goldstein, A. H., D. B. Millet, M. McKay, L. Jaegle, L. Horowitz, O. Cooper, R. Hudman, D. J. Jacob, S. Oltmans, and A. Clarke (2004), Impact of Asian emissions on observations at Trinidad Head, California, during ITCT 2K2, *J. Geophys. Res.*, *109*, D23S17, doi:10.1029/2003JD004406.

Grell, G., J. Dudhia, and D. Stauffer (1995), A description of the fifth-generation Penn State/NCAR mesoscale model (MM5), *NCAR Tech Memo. NCAR/TN-398+STR*, 117 pp., Natl. Cent. for Atmos. Res., Boulder, Colo.

Gurney, K. R., et al. (2002), Towards robust regional estimates of CO_2 sources and sinks using atmospheric transport models, *Nature*, *415*(6872), 626–630.

Haaslaursen, D. E., D. E. Hartley, and T. J. Conway (1997), Consistent sampling methods for comparing models to CO_2 flask data, *J. Geophys. Res.*, *102*(D15), 19,059–19,071.

Helliker, B. R., J. A. Berry, A. K. Betts, P. Bakwin, K. Davis, A. S. Denning, J. R. Ehleringer, J. B. Miller, M. P. Butler, and D. M. Ricciuto (2004), Estimates of net CO_2 flux by application of equilibrium boundary layer concepts to CO_2 and water vapor measurements from a tall tower, *J. Geophys. Res.*, *109*, D20106, doi:10.1029/2004JD004532.

Hong, S. Y., and H. L. Pan (1996), Nonlocal boundary layer vertical diffusion in a medium-range forecast model, *Mon. Weather Rev.*, *124*(10), 2322–2339.

Janssens, I. A., et al. (2003), Europe's terrestrial biosphere absorbs 7 to 12% of European anthropogenic CO_2 emissions, *Science*, *300*, 1538–1542.

Kalnay, E., et al. (1996), The NCEP/NCAR 40-Year Reanalysis Project, *Bull. Am. Meteorol. Soc.*, *77*(3), 437–471.

Kistler, R., et al. (2001), The NCEP-NCAR 50-year reanalysis: Monthly means CD-ROM and documentation, *Bull. Am. Meteorol. Soc.*, *82*(2), 247–267.

Lalas, D. P., D. N. Asimakopoulos, and D. G. Deligiorgi (1983), Sea-breeze circulation and photochemical pollution in Athens, Greece, *Atmos. Environ.*, *17*, 1621–1632.

Law, B. E., D. Turner, J. Campbell, O. J. Sun, S. Van Tuyl, W. D. Ritts, and W. B. Cohen (2004), Disturbance and climate effects on carbon stocks and fluxes across Western Oregon USA, *Global Change Biol.*, *10*(9), 1429–1444.

Lea, D. A. (1968), Vertical ozone distribution in the lower troposphere near an urban pollution complex, *J. Appl. Meteorol.*, *7*, 252–265.

Lu, R., and R. P. Turco (1994), Air pollutant transport in a coastal environment: 1. Two-dimensional simulations of sea-breeze and mountain effects, *J. Atmos. Sci.*, *51*(15), 2285–2308.

Lu, R., and R. P. Turco (1995), Air pollutant transport in a coastal environment: 2. Three-dimensional simulations over Los Angeles Basin, *Atmos. Environ.*, *29*(13), 1499–1518.

Lueker, T. J. (2004), Coastal upwelling fluxes of O_2, N_2O, and CO_2 assessed from continuous atmospheric observations at Trinidad, California, *Biogeosciences*, *1*, 101–111.

Lueker, T. J., R. F. Keeling, and M. K. Dubey (2001), The oxygen to carbon dioxide ratios observed in emissions from a wildfire in Northern California, *Geophys. Res. Lett.*, *28*(12), 2413–2416.

Lueker, T. J., S. J. Walker, M. K. Vollmer, R. F. Keeling, C. D. Nevison, R. F. Weiss, and H. E. Garcia (2003), Coastal upwelling air-sea fluxes revealed in atmospheric observations of O_2/N_2, CO_2 and N_2O, *Geophys. Res. Lett.*, *30*(6), 1292, doi:10.1029/2002GL016615.

Manins, P. C. (1992), Vertical fluxes in katabatic flows, *Boundary Layer Meteorol.*, *60*, 169–178.

Masarie, K. A., and P. P. Tans (1995), Extension and integration of atmospheric carbon-dioxide data into a globally consistent measurement record, *J. Geophys. Res.*, *100*(D6), 11,593–11,610.

McElroy, J. L., and T. B. Smith (1986), Vertical pollutant distributions and boundary layer structure observed by airborne lidar near the complex southern California coastline, *Atmos. Environ.*, *20*, 1555–1566.

McElroy, J. L., and T. B. Smith (1991), Lidar descriptions of the mixing-layer thickness characteristics in a complex terrain/coastal environment, *J. Appl. Meteorol.*, *30*, 585–597.

Millet, D. B., et al. (2004), Volatile organic compound measurements at Trinidad Head, California, during ITCT 2K2: Analysis of sources, atmospheric composition, and aerosol residence times, *J. Geophys. Res.*, *109*, D23S16, doi:10.1029/2003JD004026.

Olsen, S. C., and J. T. Randerson (2004), Differences between surface and column atmospheric CO_2 and implications for carbon cycle research, *J. Geophys. Res.*, *109*, D02301, doi:10.1029/2003JD003968.

Peterson, J., W. Komhyr, T. Harris, and L. Waterman (1982), Atmospheric carbon-dioxide measurements at Barrow, Alaska, 1973–1979, *Tellus*, *34*, 166–175.

Peterson, J., W. Komhyr, L. Waterman, R. Gammon, K. Thoning, and T. Conway (1986), Atmospheric CO_2 variations at Barrow, Alaska, 1973–1982, *J. Atmos. Chem.*, *4*, 491–510.

Poulos, G. S., and J. E. Bossert (1995), An observational and prognostic numerical investigation of complex terrain dispersion, *J. Appl. Meteorol.*, *34*, 650–669.

Poulos, G. S., J. E. Bossert, T. B. McKee, and R. A. Pielke (2000), The interaction of katabatic flow and mountain waves: Part I. Observations and idealized simulations, *J. Atmos. Sci.*, *57*(12), 1919–1936.

Prinn, R. G., et al. (2000), A history of chemically and radiatively important gases in air deduced from ALE/GAGE/AGAGE, *J. Geophys. Res.*, *105*(D14), 17,751–17,792.

Ramonet, M., and P. Monfray (1996), CO_2 baseline concept in 3-D atmospheric transport models, *Tellus, Ser. B*, *48*, 502–520.

Riley, W. J., C. J. Still, B. R. Helliker, M. Ribas-Carbo, and J. A. Berry (2003), ^{18}O composition of CO_2 and H_2O ecosystem pools and fluxes in a tallgrass prairie: Simulations and comparisons to measurements, *Global Change Biol.*, *9*(11), 1567–1581.

Saleska, S. R., et al. (2003), Carbon in Amazon forests: Unexpected seasonal fluxes and disturbance-induced losses, *Science*, *302*, 1554–1557.

Sellers, P. J., D. A. Randall, C. J. Collatz, J. A. Berry, C. B. Field, D. A. Dazlich, C. Zhang, and G. D. Colello (1996), A revised land surface parameterization (SiB2) for atmospheric GCMs: Part 1. Model formulation, *J. Clim.*, *9*, 676–705.

Stull, R. B. (1988), *An Introduction to Boundary Layer Meteorology*, 666 pp., Springer, New York.

Tans, P., I. Fung, and T. Takahashi (1990), Observational constraints on the global atmospheric carbon dioxide budget, *Science*, *247*, 1431–1443.

Whittlestone, S., E. Robinson, and S. Ryan (1992), Radon at the Mauna Loa observatory: Transport from distant continents, *Atmos. Environ., Part A*, *26*, 251–260.

Whittlestone, S., S. D. Schery, and Y. Li (1996), Pb-212 as a tracer for local influence on air samples at Mauna Loa observatory, Hawaii, *J. Geophys. Res.*, *101*(D9), 14,777–14,785.

Yi, C. X., K. J. Davis, B. W. Berger, and P. S. Bakwin (2001), Long-term observations of the dynamics of the continental planetary boundary layer, *J. Atmos. Sci.*, *58*(10), 1288–1299.

P. N. Foster, Department of Earth Sciences, University of Bristol, Wills Memorial Building, Queen's Road, Bristol BS8 1RJ, UK. (prufoster@yahoo.com)

T. J. Lueker, Geosciences Research Division, Scripps Institution of Oceanography, La Jolla, CA 92093-0244, USA. (tlueker@ucsd.edu)

J. T. Randerson, Earth System Science Department, 3212 Croul Hall, University of California, Irvine, CA 92697, USA. (jranders@uci.edu)

W. J. Riley, Earth Sciences Division, E.O. Lawrence Berkeley National Laboratory, 90-1106, 1 Cyclotron Rd, Berkeley, CA 94720, USA. (wjriley@lbl.gov)